Snapp et al. *NPG Asia Materials* (2020) 12:22
https://doi.org/10.1038/s41427-020-0203-1

NPG Asia Materials

REVIEW ARTICLE Open Access

Interaction of 2D materials with liquids: wettability, electrochemical properties, friction, and emerging directions

Peter Snapp[1], Jin Myung Kim[2], Chullhee Cho[1], Juyoung Leem[1], Md Farhadul Haque[1] and SungWoo Nam[1,2]

Abstract

The emergence of two-dimensional (2D) materials as functional surfaces for sensing, electronics, mechanics, and other myriad applications underscores the importance of understanding 2D material–liquid interactions. The thinness and environmental sensitivity of 2D materials induce novel surface forces that drive liquid interactions. This complexity makes fundamental 2D material–liquid interactions variable. In this review, we discuss the (1) wettability, (2) electrical double layer (EDL) structure, and (3) frictional interactions originating from 2D material–liquid interactions. While many 2D materials are inherently hydrophilic, their wettability is perturbed by their substrate and contaminants, which can shift the contact angle. This modulation of the wetting behavior enables templating, filtration, and actuation. Similarly, the inherent EDL at 2D material–liquid interfaces is easily perturbed. This EDL modulation partially explains the wettability modulation and enables distinctive electrofluidic systems, including supercapacitors, energy harvesters, microfluidic sensors, and nanojunction gating devices. Furthermore, nanoconfinement of liquid molecules at 2D material surfaces arising from a perturbed liquid structure results in distinctive hydrofrictional behavior, influencing the use of 2D materials in microchannels. We expect 2D material–liquid interactions to inform future fields of study, including modulation of the chemical reactivity of 2D materials via tuning 2D material–liquid interactions. Overall, 2D material–liquid interactions are a rich area for research that enables the unique tuning of surface properties, electrical and mechanical interactions, and chemistry.

Origin of 2D material interactions with liquids

The ideal interaction between a surface and a liquid is dictated by surface forces. Surface forces can be subdivided into three components: van der Waals forces, which exist at any interface between solids and liquids; electrostatic interactions, which exist between charged or polar surfaces and fluids; and structural forces, principally hydrogen bonding[1]. These interactions influence the wetting behavior and determine whether the interaction with water is hydrophilic or hydrophobic, control the electronic structure at the liquid–solid interface, influence the frictional interaction, and modulate the chemical activity. However, this ideal picture of the surface interactions is complicated when considering surface heterogeneities, including roughness[2] and contamination[3], which interfere with the formation of an equilibrium configuration between the liquid and the surface, leading to eccentric behaviors, including superwetting, superslipping, and superhydrophobicity. These surface heterogeneities also allow the surface liquid interactions to be tuned, enabling an array of applications in sensing, chemical transport, and actuation. Two-dimensional (2D) materials, which are extremely thin, have unique electrical properties, and have a tendency to deform and accumulate contamination during processing, resulting in unique

Correspondence: Peter Snapp (knapp7@illinois.edu) or SungWoo Nam (swnam@illinois.edu)
[1]Department of Mechanical Science and Engineering, University of Illinois at Urbana-Champaign, Urbana, IL 61801, USA
[2]Department of Materials Science and Engineering, University of Illinois at Urbana-Champaign, Urbana, IL 61801, USA
These authors contributed equally: Peter Snapp, Jin Myung Kim, Chullhee Cho

surface forces and heterogeneities that lead to novel surface liquid interactions.

Temporarily confining the discussion to graphene, a well-known 2D form of carbon that demonstrates surface behaviors which are representative of those of the large family of 2D materials, one can begin to understand the complex interactions between a liquid and a 2D material surface. Graphene demonstrates long-range π conjugation[4], resulting in unique surface and chemical properties. For example, graphene interacts with molecules that are weakly adsorbed on its surface by donating or accepting charge carriers, resulting in a modulation of carrier concentration or doping[4]. This interaction is further complicated by the influence of underlying substrates, which also have doping effects[5], and is highly dependent on the ambient environment and the number of layers making up the graphene film[4]. Furthermore, the inherent thinness of graphene, and indeed all 2D materials, causes 2D materials to exhibit out-of-plane morphologies, i.e., roughness, folds, and ripples, that arise from 2D materials' vanishing flexural rigidity[6] and causes an extreme sensitivity to surface contamination[3], further complicating the interaction between a graphene surface and a liquid.

Wettability of 2D materials

Inherent wettability of 2D materials

The most basic interaction between a surface and a liquid is wetting, where a balance between adhesive and cohesive forces controls the geometry of the liquid spreading across a surface. Focusing on the simple wetting of unmodified graphene with water, there is longstanding and ongoing debate as to whether graphene is inherently hydrophobic or hydrophilic. The earliest measurements of the wettability of natural graphite, highly oriented pyrolytic graphite (HOPG) which is essentially graphene with many layers, and single-layer graphene all yielded water contact angles (WCAs) at or above 90° and led to the early conclusion that all graphitic materials are hydrophobic[7]. These results have been consistently reproduced since the 1940s for graphene produced by a variety of methods[7]. Measurements of WCAs on graphene oxide and graphite flakes produced using a hydrazine reduction method indicated that while the source graphene oxide was hydrophilic with a surface energy of 62.1 mJ/m^2, the produced graphene was hydrophobic with a surface energy of 46.7 mJ/m^2, which lent credence to the conclusion that graphene is intrinsically hydrophobic[8]. Measurements of the advancing and receding WCA as a function of the number of layers of graphene over a suspended substrate, supplemented with molecular dynamics (MD) simulation, complicate the conclusions slightly but still indicate that at least the advancing WCA of graphene is consistent with that of 3D bulk graphite (~90°) regardless of the substrate or number of layers, further reinforcing the idea that graphene is intrinsically hydrophobic[9]. However, previous works[9] did observe inconsistencies in receding WCA and contact angle hysteresis, which they attributed to defects in their as-grown and transferred graphene sheets.

Despite the substantial amount of data indicating that graphene is hydrophobic, evidence is growing that suggests that this picture might be flawed. At this point, it is instructive to examine the basic chemical nature of graphene, which can be considered an extended polycyclic aromatic hydrocarbon. The base unit of any polycyclic aromatic hydrocarbon is the benzene ring, and therefore, it is possible to draw parallels between the interaction of benzene with water and the interaction of graphene with water. We focus on the interaction of water molecules located above the benzene plane, which is more representative of the interaction of water with the basal plane of graphene. Ground-state microwave spectra of jet cooled clusters of benzene and water were used to determine the geometry of a water molecule interacting with the plane of a benzene molecule. Subsequent ab initio calculations based on this geometry indicated that benzene acts as a hydrogen bond acceptor and that aromatic hydrophilic attraction should be reflected in similar structures across nature, including graphene[10].

This predicted hydrophilic interaction was reflected in subsequent studies of graphitic carbon-water nonbonded interactions. Ab initio calculations, random-phase approximations, density functional theory (DFT) symmetry-adapted perturbation theory, and coupled cluster treatment yield interaction energies and distances between the polycyclic aromatic hydrocarbon (PAH) plane and the oxygen atom of an interacting water molecule[11] that were consistent with those experimentally determined and calculated for benzene[10] (interaction energy of ~3 kcal/mol and oxygen-PAH separation of ~3 Å). These interaction parameters informed molecular dynamics simulations that indicate graphene demonstrates hydrophilic interactions with a WCA that decreased as the number of simulated graphene layers increased (Fig. 1a)[11]. Furthermore, the DFT simulation was extended to incorporate the effect of changing the water molecule configuration and charging of the graphene to simulate doping. These simulations demonstrated that while simulated doping led to a modification of the water molecule orientation, it also promoted an increased interaction between the graphene and water, enhancing graphene's hydrophilicity. Complementary examination of the WCA on biased graphene and the condensation of water on chemically doped graphene further indicated that graphene is inherently hydrophilic, but hydrophilicity is sensitive to Fermi level changes and is tunable via doping[12], which is discussed in depth later in this review.

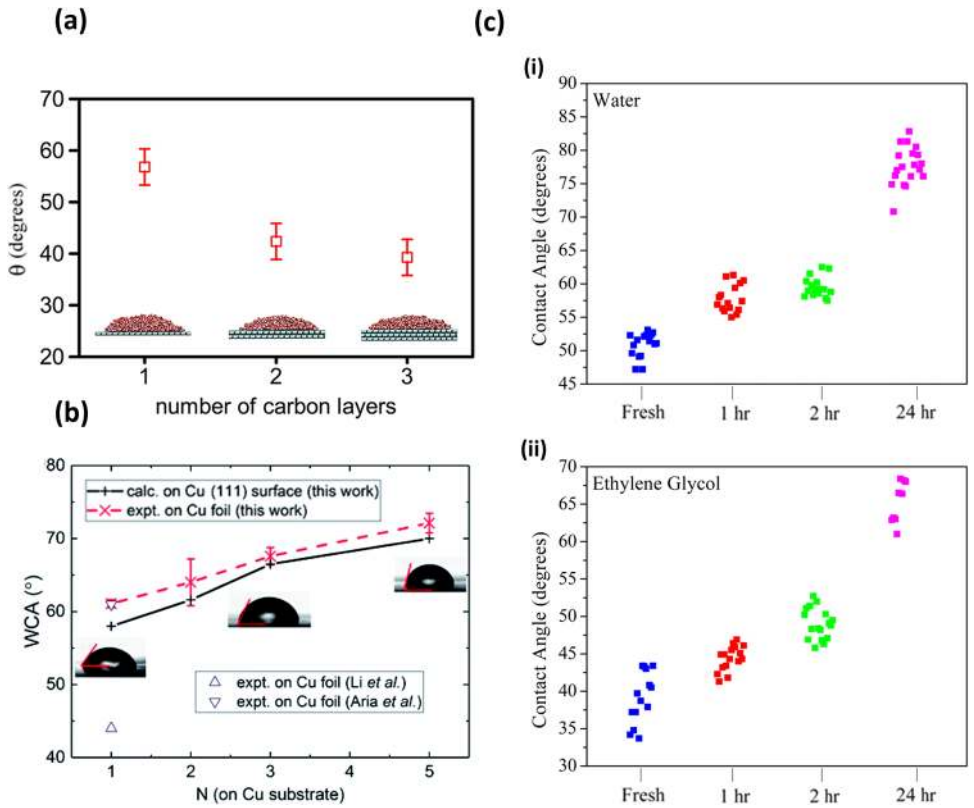

Fig. 1 Intrinsic wettability of 2D materials. a Dependence of the WCA on the number of carbon layers (as determined by ab initio calculation)[11]. **b** Calculated and measured WCA as a function of the number of graphene layers (N) on the Cu substrate[13]. **c** Contact angle data on graphene/Cu for (i) water and (ii) ethylene glycol. All data were taken at the times indicated on the *x*-axis and are shifted horizontally in the figures for clarity[19]. **a** Reprinted (adapted) with permission from Wu and Aluru[11], Copyright (2013) American Chemical Society. **b** Reproduced with permission from Liu et al.[13], published by The Royal Society of Chemistry. **c** Reproduced with permission from ACS (Kozbial et al.)[19]. Available at (https://pubs.acs.org/doi/abs/10.1021/la5018328); further permission related to the excerpted material should be directed to the ACS.

This picture of graphene being inherently hydrophilic and perturbed by its environment is in fact widely reported and is now a benchmark for the accuracy of a proposed WCA measurement or calculation technique, which in the case of graphene on copper, should yield a WCA near 60° that increases with an increasing number of graphene layers (Fig. 1b)[13]. Liu et al. offered a broad overview of these works[14]. Condensing key findings that indicated that graphene is inherently hydrophilic, it was found that freshly prepared samples of graphene and graphite demonstrated WCAs of 42° and 64°, respectively, indicating intrinsic hydrophilicity. Similar results were observed in subsequent studies, where a freshly cleaved HOPG sample demonstrated a WCA of 62° indicative of inherent hydrophilicity. Moving away from WCA measurements, direct measurements of the surface energy of graphene using a modified surface force balance utilizing a crossed-cylinder single-contact geometry indicated that the interfacial energy between few-layer graphene (FLG) and water (83 ± 7 mJ/m^2) is lower than the FLG surface energy (119 ± 3 mJ/m^2)[15], which in the context of the Young equation, implies hydrophilic behavior. Similarly, when considering computational studies of the interaction between water and graphene, most simulations indicate that the preferred adsorption orientation for water over graphene is hydrogen pointing into the graphene lattice, indicating that π-hydrogen bonding is likely responsible for the inherent hydrophilicity[14,16]. This is not to say that the question of the inherent wettability of graphene has been settled, as recent works still maintain that graphene is hydrophobic[17], but that there is compelling evidence that graphene may be inherently hydrophilic.

However, rigidly defining graphene or any 2D material as hydrophobic or hydrophilic is not fruitful. While pristine, isolated graphene interacting with isolated pure water molecules may demonstrate intrinsic hydrophilicity[11], the complex interaction between graphene and its environment, defects, and contamination means that the hydrophilicity of graphene needs to be considered on a case-by-case basis[13]. Indeed, given the extensive ability to enrich the functionality of graphene and other 2D

materials by surface engineering, it is far more reasonable to address the specific effect of the 2D material's environment, i.e., its substrate, surface chemical composition, doping, charge/electric field, and crystallinity/topography, on the 2D material's wettability.

It is worth discussing nongraphene 2D materials at this point. While an in-depth discussion of the intrinsic and in situ wettability of every member of the growing family of 2D materials is beyond the scope of this review, it is worth noting consistent parallels between wettability measurements of graphene and other 2D materials. Focusing on 2D transition metal dichalcogenides (TMDCs), specifically molybdenum disulfide (MoS_2), one again observes that clean, isolated MoS_2 demonstrates hydrophilic behavior (WCA of 69.0 ± 3.8°) but the behavior transitions to hydrophobic (WCA of 89.0 ± 3.1°) under ambient conditions[18]. This indicates that the disruption of the intrinsic wetting behavior of 2D materials by their environment is universal and is likely to be observed in 2D hexagonal boron nitride (h-BN), MXenes, and indeed any atomically thin material regardless of intrinsic wettability. In a similar vein, while a discussion of the interaction of every available solvent with graphene is beyond the scope of this work, the perturbation of the contact angle on graphene over time is observed with a variety of solvents, including water (Fig. 1c (i)), diiodomethane, ethylene glycol (Fig. 1c (ii)), and glycerol, further reinforcing the universality of the disruption of intrinsic wetting behavior[19].

Intrinsic perturbation of the wetting behavior of 2D materials

Focusing on perturbations to the intrinsic wettability of graphene, we begin with a discussion of the effect of the substrate on the wettability of graphene. Given the extreme thinness of graphene, it was predicted that the surface force of the substrate is likely to penetrate through the graphene layer, resulting in "wetting transparency"[20]. It was subsequently reported that wetting transparency was observed on silicon and gold, where the presence of a monolayer of graphene on the surface had a minimal effect on the experimentally measured WCAs. This experimental result was reflected in complementary MD simulations[20]. However, transparency is not universal, and measurements on graphene transferred to copper and SiO_2 surfaces demonstrated a dramatic shift in the WCA (~0° to >90° in the case of graphene on copper[9]) upon the transfer of a single layer of graphene[21]. It is in fact appropriate to refer to graphene as "wetting translucent" with the relative translucency depending on the thickness of the graphene layer and the surface forces dominating the wetting behavior of the substrate. The most apparent effect of this translucency is the failure to transmit superhydrophobicity (or superhydrophilicity) through a graphene layer, as the highest achievable WCA on flat graphene is estimated to be ~96° (Fig. 2a (i)). This was confirmed by the observation of the WCAs on graphene that was transferred to superhydrophobic/superhydrophilic substrates (Fig. 2a (ii))[22], although subsequent studies emphasize the importance of completely modeling the factors influencing graphene wettability, including the bulk modulus and roughness, which markedly increase the maximum WCA[17]. Translucency is not limited to damping of the extremes of hydrophilicity/hydrophobicity but extends to the modulation of the surface forces from the 2D materials' substrates. Specifically, it was shown that dispersive dominant graphene, MoS_2, and tungsten disulfide (WS_2) develop a nonnegligible but weakened polar nature after transfer to strongly polar h-BN surfaces (Fig. 2b)[23]. This dominance of the polarity in governing the wetting translucency has repeatedly been affirmed using DFT simulation[24] and high-resolution surface probing techniques[25]. Highly polar substrates very effectively penetrate 2D materials and highly polar 2D materials, h-BN in particular, dominate liquid interactions and damp transparency. Translucency is further modulated by the number of layers of the 2D material. In the case of WS_2 and MoS_2 deposited on Si/SiO_2 substrates, the WCA approaches that of bulk WS_2 and MoS_2 after the transfer of only three layers of material (Fig. 2c)[26].

Contamination has an equally profound effect on the wettability of 2D materials. Given that all atoms of a 2D material are located at or extremely near the surface, even a minor amount of adsorbed contaminants strongly modulates the wetting. Reactive adsorbates, such as O_2, can induce charge doping. This type of doping is indicated by a shift of the G-peak position to high wavenumbers during Raman measurements of graphene exposed to dry O_2, and occurs because of an electron transfer from trapped O_2 under the graphene layer. This charge transfer leads to the development of a negatively charged adsorbate layer over graphene, which should modulate its wettability[27]. Physisorbed water, both on the graphene surface and trapped under the graphene layer, amplifies the doping effect of oxygen, resulting in permanent shifts of the G-peak during Raman measurement and amplifying any observed shift in the wettability[27]. Recent studies integrating fourier transform infrared spectroscopy (FTIR), atomic force microscopy (AFM), and static WCA measurements with DFT-predicted WCAs and DFT AFM force simulations predict the formation of ice-like water layers on top of graphene under ambient conditions (Fig. 2d (i)), which results in the hydrophobicity increasing over time (Fig. 2d (ii))[28]. Nonreactive adventitious hydrocarbons absorbed from the air also modulate the wettability of 2D materials. Li et al. reported that the WCA of freshly prepared chemical vapor deposition (CVD)-grown graphene (supported on a Cu foil) was

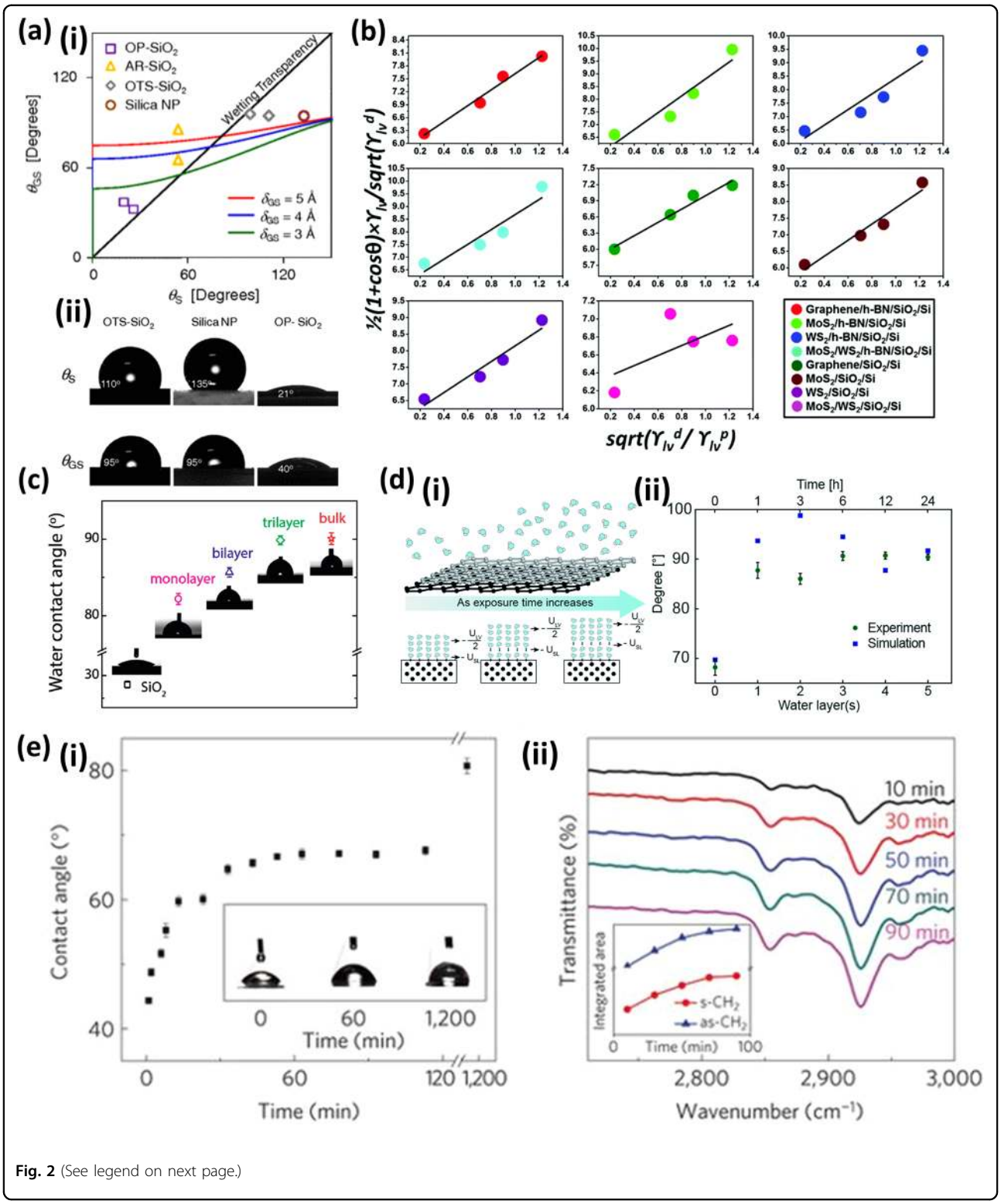

Fig. 2 (See legend on next page.)

~42°, which is consistent with the predicted hydrophilicity of graphene. The WCA then proceeded to slowly increase, plateauing at 80° after ~20 h (Fig. 2e (i)). Based on the observation that peaks in attenuated total reflectance Fourier transform infrared (ATR-FTIR) spectra indicated an increasing methylene group presence over time and X-ray photoelectron spectroscopy (XPS) peaks were consistent with carbon contamination, Li et al. attributed

(see figure on previous page)

Fig. 2 Intrinsic perturbations to the wettability of 2D materials. a (i) Calculated θ_{GS} (WCA on the graphene-coated substrate) as a function of θ_S (WCA on an uncoated substrate) for the three values of δ_{SG} (equilibrium contact separation between liquid and graphene) that were considered (colored curves) and experimentally measured values of θ_{GS} and θ_S on various substrates (colored symbols). The trend for $\theta_{GS} = \theta_s$ (black line), which corresponds to the wetting transparency, is shown as a reference. (ii) Photographs of water drops and measured values of θ_S and θ_{GS} on an octadecyltrichlorosilane (OTS)-SiO_2, silica NP (silica nanoparticles on glass), or OP-SiO_2 (oxygen plasma cleaned SiO_2) substrate with and without a sheet of monolayer graphene between them[22]. **b** Surface energy (polar and dispersive) graphs obtained for various samples based on the Owen, Wendt, Rabel and Kaelble (OWRK) model, where γ_{sl} corresponds to the liquid surface tension; γ^D and γ^P refer to the dispersive and polar components of surface tension, respectively; and θ corresponds to the WCA[23]. **c** Advancing WCA measurements for the WS_2 films with varying numbers of layers on a Si/SiO_2 substrate[26]. **d** (i) Time-resolved schematic of the water adsorption on the graphite surface in an ambient environment. (ii) Comparison of the time-resolved DFT-predicted WCAs on graphite surfaces with different numbers of adsorbed water layers and experimentally measured static WCAs with different aging times[28]. **e** (i) Temporal evolution of the WCA measured on a graphene/copper sample. The sample was removed from the CVD chamber at time 0. The three photographs show the water drops captured at 1, 60, and 1200 min. (ii) ATR-FTIR spectrum of a graphene/copper sample. The spectra were shifted vertically for clarity. The sample was removed from the CVD chamber at time 0. The inset shows the integrated peak area versus time for the peaks at 2930 cm^{-1} (asymmetric CH_2 stretching, blue) and 2850 cm^{-1} (symmetric CH_2 stretching, red)[3]. **a** Reprinted Fig. 3 with permission from Shih et al.[22], Copyright (2012) by the American Physical Society (10.1103/PhysRevLett.109.176101). **b** Republished with permission from RSC Pub. from (Annamalai et al[23].), permission conveyed through the Copyright Clearance Center, Inc. **c** Reprinted (adapted) with permission from Chow et al.[26], Copyright (2015) American Chemical Society. **d** Republished with permission from the Royal Society of Chemistry from Lu et al.[28], permission conveyed through the Copyright Clearance Center, Inc. **e** Reprinted with permission from the Copywright Clearance Center: Springer Nature, Nature Materials (Li et al[3].), Copyright (2013).

this shift to accumulated hydrocarbons (Fig. 2e (ii))[3]. This proposed hydrocarbon accumulation was further confirmed by XPS and time-of-flight secondary ion mass spectrometry (ToF-SIMS) conducted on cleaved samples of HOPG stored under different conditions, which showed the appearance of multiple hydrocarbon contaminant peaks for the HOPG stored in air[29]. The almost immediate increase in the WCA attributed to hydrocarbon absorption is now considered responsible for the early reports claiming that graphene is inherently hydrophobic[30].

Extrinsic tuning of the wettability of 2D materials

With a complete understanding of the perturbations to the wettability of graphene, it is possible to extrinsically tune its wetting behavior. Inspired by the modulation of the wetting from graphene-substrate and graphene-contamination interactions, considerable effort has been expended on understanding the effect of doping on wettability. The WCA of graphene on SiO_2 is known to correlate with the degree of p-doping, as the WCA decreased on substrates subject to pretreatment, which increased the hole concentration (O_2 plasma and UV ozone treatments)[5]. Ashraf et al. demonstrated explicit control of the WCA of graphene through Fermi level modulation by doping (Fig. 3a (i)) with subsurface polyelectrolytes changing WCA by as much as 13° with a 300 meV change in the work function that was achieved by p or n doping (Fig. 3a (ii))[31]. This modulation of the wettability by doping is attributed to the synergistic effect of a change in the 2D material surface energy, reorientation of liquid molecules near the interface, and perturbation of the formation of an electrical double layer (EDL). MD simulations indicate that modified Columbic interactions arising from doping-induced reorientation of water molecules are primarily responsible for interfacial energy changes. Furthermore, the polarity of the 2D material and the wetting liquid can induce asymmetry in the interfacial energy change. The molecular density of the first water layer adjacent to graphene increases with slight p-doping, decreasing the interfacial energy, while the molecular density decreases with slight n-doping, increasing the interfacial energy. This tunability is predicted to be observed across a variety of 2D materials and is expected to be stronger on 2D semiconductors (TMDCs) than the observed tuning on semimetals (graphene) due to the increased quantum capacitance of 2D semiconductors[32]. The modulation of wetting by doping is further influenced by reshaping the EDL, which is discussed at length later in this review[32].

Electric fields can similarly be utilized to modulate the wettability of 2D materials, enabling the instantaneous and reversible tuning of the WCA. Fundamentally, the modulation of wetting by a direct electric field is governed by a reorientation of the water molecules. High electric fields increase the number of hydrogen bonds per water molecule in the graphene interfacial region, decreasing the WCA. However, the degree of modulation is also highly dependent on the field orientation relative to the graphene surface, where perpendicular electric fields result in a minimal modulation of the interfacial structure while parallel electric fields (Fig. 3b (i–iii)) significantly increase the water spreading speed, resulting in a rapid decrease in droplet height with increasing time and field (Fig. 3b (iv))[33]. The modulation of the WCA on 2D materials by an electric field can also be achieved through electrowetting effects, in which a charge explicitly interacts with the interfacial liquid and surface energies to reduce the WCA. Applying a Teflon layer over graphene to induce initial hydrophobicity enabled the production of flexible electrowetting on

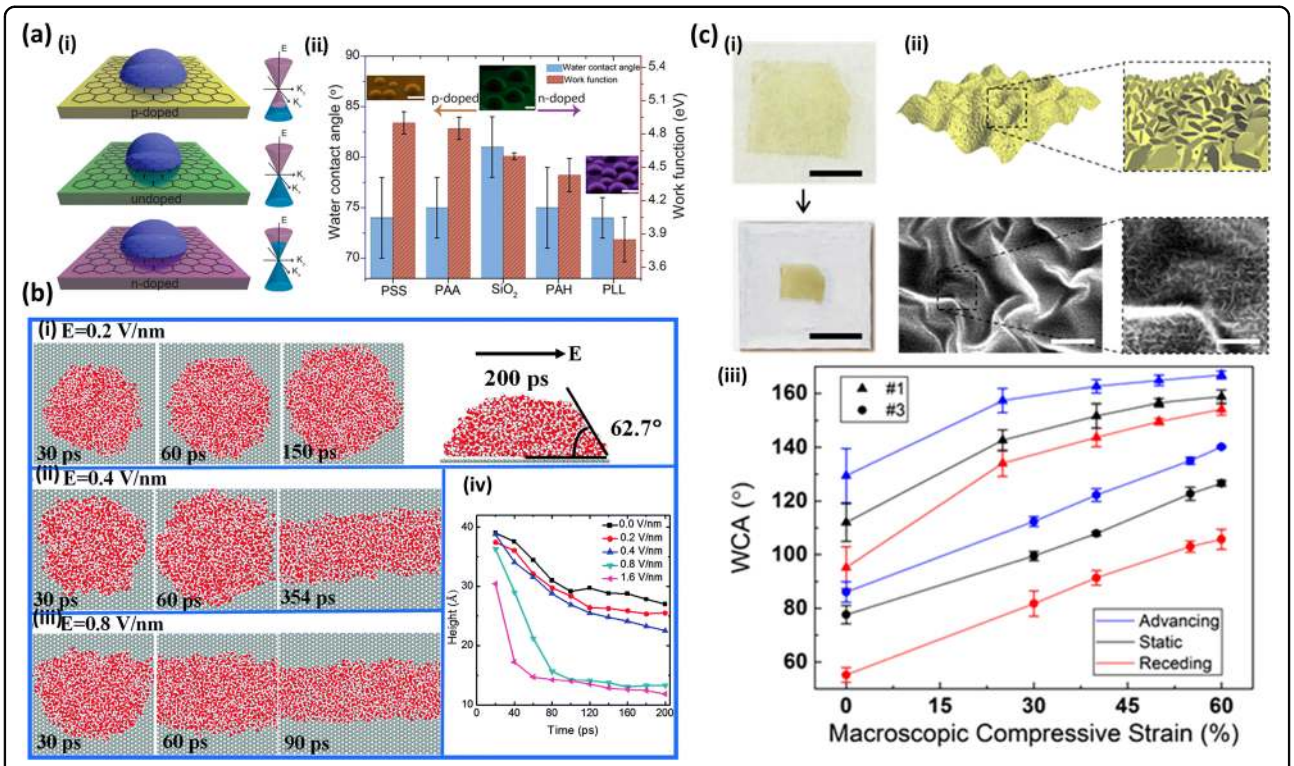

Fig. 3 Extrinsic tuning of wettability. a (i) Schematic illustration showing graphene wettability modulation by doping-induced Fermi level shifts. (ii) WCA (left axis) measured by environmental scanning electron microscopy (E-SEM) and work function (WF, right axis) measured by scanning Kelvin probe microscopy (SKPM) of polyelectrolyte-doped and undoped graphene samples. For both n- and p-doping, the WCA of the graphene decreases. Insets show false-colored E-SEM images of the water droplets (scale bars represent 10 μm)[31]. **b** Snapshots of the water droplet spreading process under an electric field parallel to the graphene surface at (i) $E = 0.2\,\mathrm{V\,nm^{-1}}$, (ii) $E = 0.4\,\mathrm{V\,nm^{-1}}$, and (iii) $E = 0.8\,\mathrm{V\,nm^{-1}}$. The equilibrium system possesses a WCA of 62.7° at $E = 0.2\,\mathrm{V\,nm^{-1}}$. (iv) The height of the water droplets versus simulation time under various electric fields[33]. **c** The tunable wettability of MoS_2 nanoflowers by manipulation of the microstructure. (i) Photos of as-transferred (upper panel) and crumpled (lower panel) MoS_2 nanoflowers on a polystyrene (PS) substrate. Scale bars: 1 cm. (ii) Schematic illustrations (upper panel) and SEM images (lower panel) of crumpled MoS_2 nanoflowers via thermal shrinkage of a PS substrate. Scale bars: 500 nm (lower left) and 100 nm (lower right). (iii) Tunable advancing/static/receding WCAs of MoS_2 nanoflowers as a function of macroscopic compressive strain. Triangles denote the #1 nanoflowers (the roughest), whereas circles represent the #3 nanoflowers (the flattest)[40]. **a** Reprinted (adapted) with permission from Ashraf et al.[31], Copyright (2016) American Chemical Society. **b** Republished with permission from the Royal Society of Chemistry from Ren et al.[33], permission conveyed through the Copyright Clearance Center, Inc. **c** Reprinted (adapted) with permission from Choi et al.[40], Copyright (2017) American Chemical Society.

dielectric (EWOD) actuators that modulate the WCA reversibly by up to 30° with application of a 0–40 V AC bias[34]. It is possible to avoid the use of a Teflon layer on top of graphene and induce hydrophobicity by increasing the graphene roughness, which allows the direct application of graphene to create surfaces suitable for electrowetting modulation without subsequent application of a hydrophobic polymer layer[35]. Sophisticated control of wetting is possible by coupling electrical and thermal effects. MD simulations indicate that increasing the temperature results in a linear reduction in the WCA that can then be reversed by increasing the charge magnitude, enabling a hydrophilic to hydrophobic transition[36].

In addition to modulating the wetting through doping and an electrical field, it is also possible to tune the wettability through reversible chemical decoration of the graphene surface. The application of carbonyl, hydroxyl, or epoxy groups that are either chemically bound or physiosorbed to the graphene, or indeed any 2D material, surface allows for the transition from hydrophobicity to hydrophilicity. Cyclic exposure to a low and high pH (2–12) solution is a facile method to manipulate the population of these surface moieties. Creating acidic or basic conditions drives protonation or deprotonation respectively, and therefore reversibly tunes the wettability from hydrophobic (pH 2–6) to hydrophilic (pH 8–12)[37]. Similarly, exposure to ultraviolet radiation causes dissociative absorption of water on the surface of graphene, which decorates the graphene surface with hydrophilic groups and reduces the WCA. This modulation of the WCA is reversible by subsequent aging in a vacuum, which permits desorption of the adsorbed groups, causing the WCA to return to its initial value[38].

It is also possible to tune the wettability by directly modifying the structure of a 2D material, which changes the exposure of surface features as well as the roughness. 2D TMDCs, such as MoS_2, demonstrate a large variation in their surface morphology depending on the synthesis conditions. Specifically, MoS_2 exhibits an increasing WCA with increasing temperature during chemical vapor deposition[39]. This hydrophilic to hydrophobic transition is attributed to an increased presence of defects/vacancies in MoS_2 synthesized at low temperatures, as observed with transmission electron microscopy and Raman spectroscopy. Defects expose active edge sites that increase the free energy and therefore lead to improved wetting, indicating that varying the crystallinity of 2D films can modulate their wetting behavior[39]. It is further possible to actively tune morphology's influence on wetting by coupling the topography to external stimuli, including strain. Structures utilizing nanoflower MoS_2 were deformed to produce micro/nano hierarchical structures using a substrate contraction technique (Fig. 3c (i)). The morphology of nanoflower MoS_2 has already been modified to increase the hydrophobicity through the deposition process; when this hydrophobicity is combined with the roughening effect from the wavy deformation the surface transitions to a superhydrophobic state (Fig. 3c (ii)). Increasing the compressive strain can subsequently be used to augment the deformation and increase the surface roughness and hydrophobicity (Fig. 3c (iii)). This modulation of multiscale roughness using strain-controlled deformation enabled intelligent tuning of the WCA from 80 to 155° and provided reversible modulation of the WCA over thousands of strain cycles[40].

Applications of 2D materials with tunable wettability

The controllable wettability of 2D materials enables a wide variety of applications of interest to the broad scientific community. As surfaces for biological applications, the controllable wettability of graphene allows selective adsorption and bioadhesion, allowing directed cell growth and control of the differentiation of bone cells from stem cells (Fig. 4a)[41]. It is possible to create Janus 2D materials where there is a significant mismatch in wetting properties on both sides by taking advantage of the ability to control the wettability of both sides of a 2D material (Fig. 4b), which enables separation applications, including extraction of water from oil and vice versa[42,43]. In a similar vein, varying the surface wettability, especially locally, modifies nucleation and crystal growth processes across the surface, enabling control of the orientation and spatial growth of organic films. For instance, pentacene films grown on multilayer graphene demonstrated a decreased island height (Fig. 4c (i)) and increased island lateral dimension (Fig. 4c (ii)) with an increasing number of graphene layers[44]. Furthermore, the ability to control the wettability, and therefore water permeability, of nanoporous graphene allows high water vapor transmission rates[45]. Finally, active and rapid tunability of the WCA on 2D materials enables precise control of the geometry of water on graphene for unique optical applications, including dielectrically modulated liquid lenses for compound eye applications[34].

Electrical double layer of 2D materials

When focusing specifically on the local interfacial interaction between a wetting liquid and a 2D material, it is of vital importance to discuss the formation of an EDL. EDL formation has been referred to in the previous discussion about wetting but deserves a dedicated section owing to the recent and growing interest in understanding EDL formation and effects above 2D materials. An EDL is found at the interface between charged solids and electrolytes due to Coulomb interactions between surface charges and ions, which cause exponential attenuation of the surface potential with excess counterions and deficient co-ions within the Debye length. The formation of EDLs from atomically thin materials has attracted considerable attention as EDLs have the potential to answer fundamental questions about the unique interaction of two-dimensional materials and ions and also enable electrochemical applications, including supercapacitors, energy harvesters, microfluidic/molecule sensors, and nanojunction gating devices. Thus, it is of crucial importance to understand the fundamental principles of interfacial phenomena when 2D materials are exposed to an ionic liquid environment.

From the point of view mentioned above, there have been a number of theoretical and experimental studies that closely resemble the studies on wetting described previously that consider the characteristics of EDL formation on 2D materials as a function of the substrate material, number of layers, defects, dopants, and organic contaminant layers. These studies have mainly focused on graphene-electrolyte systems. One of the unique aspects of this system is that the total capacitance of the liquid-2D material is composed of various capacitances in series (Eq. 1), and the total capacitance mainly consists of the quantum capacitance and EDL capacitance[46]. To prevent confusion regarding the notation, we define the total capacitance (C_T) as the EDL capacitance (C_{EDL}) and quantum capacitance (C_Q) and other capacitances (e.g., the dielectric screening capacitance (C_{DS}) and dielectric dead layer capacitance (C_{DL})) connected in series.

$$\frac{1}{C_T} = \frac{1}{C_{EDL}} + \frac{1}{C_Q} + \frac{1}{C_{DS}} + \frac{1}{C_{DL}} \quad (1)$$

First, the EDL capacitance of graphene is strongly affected by van der Waals forces from the underlying

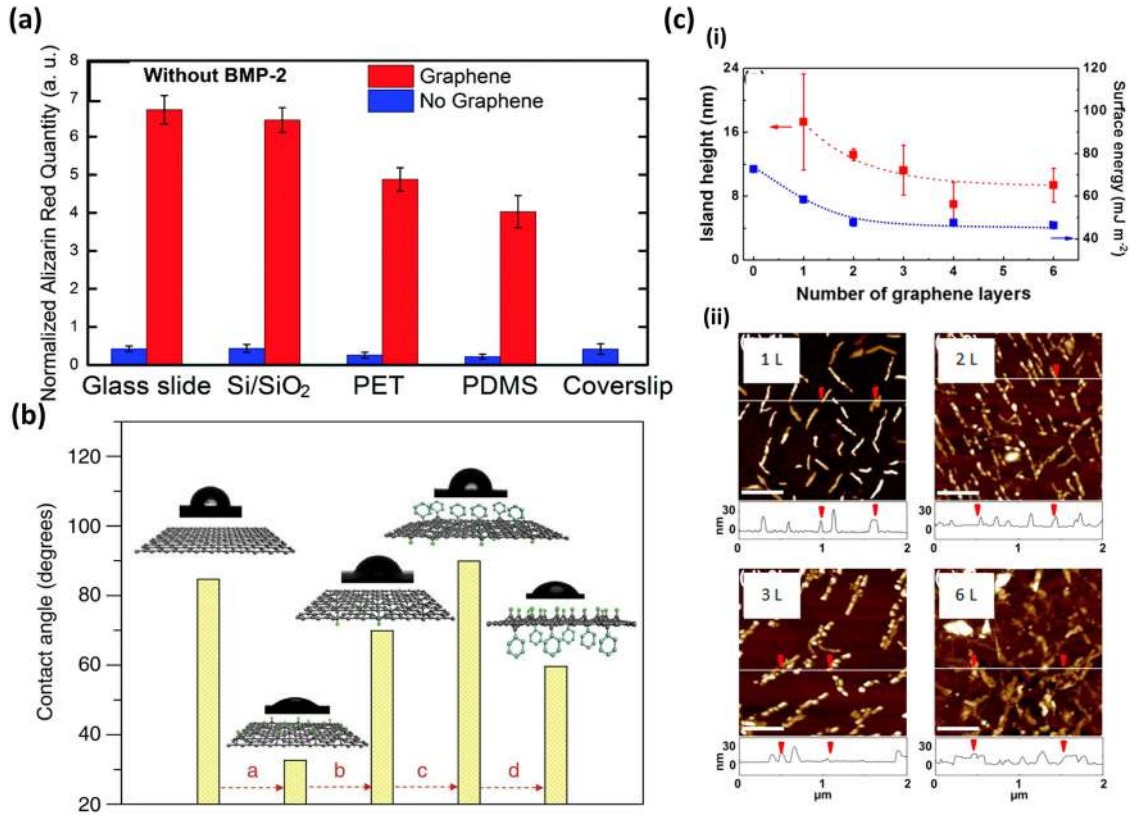

Fig. 4 Applications of wetting modulation. a Graphene accelerates osteogenic differentiation. Cells grown in the absence of BMP-2 (growth factor conventionally used to drive differentiation). The control experiment with coverslips is shown as a reference[41]. **b** Functional graphene derivative with bifacially anisotropic wettability. Static WCA measurements during the fabrication of Janus graphene: **a** single-sided photochlorination; **b** exposure of fresh (untreated) side of graphene; **c** single-sided phenylation; and **d** release of Janus graphene. The insets exhibit images of water droplets and schematic illustrations of the related surfaces of Janus graphene from asymmetric two-dimensional chemistry[42]. **c** Effect of the number of graphene layers on the substrate-pentacene interaction at the initial growth stage of pentacene. (i) Plot of the average island heights of 2 nm thick pentacene films and the surface energy of graphene-covered hydrophilic substrate versus the number of graphene layers (1−6 L). AFM images of 2 nm thick pentacene films on different numbers of graphene layers transferred onto the hydrophilic substrate. (1 L) Single layer, (2 L) two layers, (3 L) three layers, and (6 L) six layers. The scale bars are 0.5 μm[44]. **a** Reprinted (adapted) with permission from (Nayak et al.)[41], Copyright (2011) American Chemical Society. **b** Modified after (Zhang et al.)[42]. (© 2013, Nature Publishing Group) (license: https://creativecommons.org/licenses/by-nc-sa/3.0/legalcode), **c** Reprinted (adapted) with permission from Nguyen et al.[44], Copyright (2015) American Chemical Society.

substrate. Kwon et al. elucidated the effect of van der Waals interactions between a substrate and liquid through graphene by measuring the EDL capacitance of graphene on different substrates[47]. Increasing the hydrophobicity of the substrate by switching from SiO_2 to polytetrafluoroethylene (PTFE) modified the hydrogen bonding network of water molecules near the graphene, which were disturbed by the penetrating hydrophobicity of the substrate. As a consequence, the density of water molecules was reduced compared to that of the bulk liquid, and furthermore, the permittivity of the water was reduced near the surface due to disruptions in the dipole alignment. For these reasons, increasing the hydrophobicity of substrates (i.e., producing a higher WCA) causes a noticeable degradation of the EDL capacitance. Figure 5a shows that the transfer characteristics of an ion-gated graphene field-effect transistor (FET) revealed that the transconductance of graphene was inversely correlated with the hydrophobicity of its substrate because of the decreased total capacitance of graphene on a hydrophobic substrate. These experimental observations were corroborated by MD simulation, which confirmed that hydrophilic substrates induce a densely packed double layer near the graphene-water interface, while hydrophobic substrates hinder EDL formation (Fig. 5b, c). Another MD simulation from Yang et al. also demonstrated that the hydrophilicity of a substrate strongly affects the distribution of both water molecules and counter-/co-ions[48]. However, according to their calculation, total capacitances are not significantly dependent on different substrates due to changes in solvent polarization ability and screening efficiency.

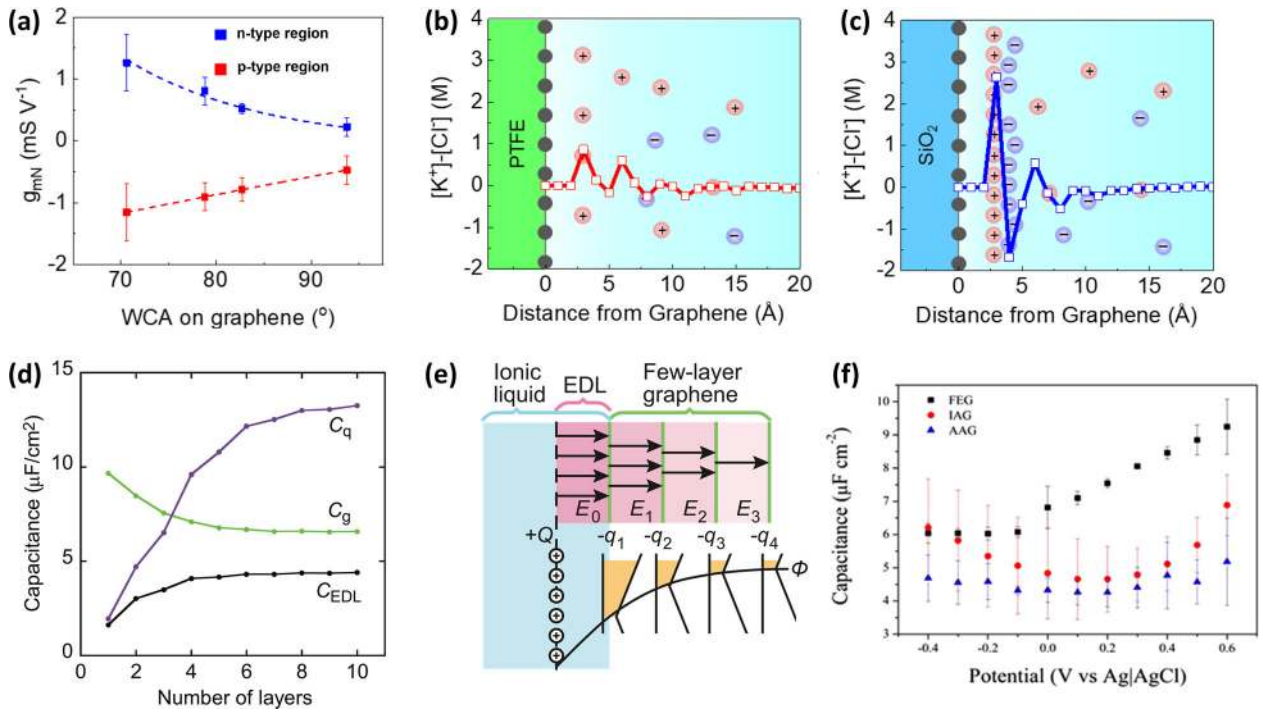

Fig. 5 Various factors that influence the formation of an EDL on a graphene surface. a Normalized transconductance at n-type and p-type regions as a function of the WCA on graphene. **b**, **c** Ion distribution calculated as a function of distance from graphene when the substrate is **b** hydrophobic PTFE and **c** hydrophilic SiO_2. Note that hydrophilic substrates induce a densely packed and well-defined electrical double layer on the graphene surface, while hydrophobic substrates suppress EDL formation[47]. **d** Changes in the total capacitance, geometrical capacitance, and quantum capacitance (denoted as C_{EDL}, C_g, and C_q, respectively) as a function of the number of layers of graphene. **e** Accumulated charge distribution over the double layer capacitor and few-layered graphene quantum capacitors[50]. **f** Total capacitance of HOPG prepared with different aging conditions, FEG for freshly exfoliated HOPG, IAG for HOPG aged in an inert-gas atmosphere, and AAG for HOPG aged in an air atmosphere[52]. **a**–**c** Reprinted (adapted) with permission from Kwon et al.[47], Copyright (2019) American Chemical Society. **d**, **e** Modified after (Uesugi et al.[50]. (© 2013, Springer Nature) (license: https://creativecommons.org/licenses/by-nc-nd/3.0/legalcode). **f** Reproduced with permission from the ACS (Zou et al.[52].), available at (10.1021/acs.langmuir.6b02910). Additional permissions related to the excerpted material should be directed to the ACS[52].

Similarly, the number of graphene layers is an important factor that determines EDL capacitance as it changes the electrostatic charge distribution and the density of states of graphene. Ji et al. reported that the total capacitance of graphene is enhanced by decreasing the number of graphene layers when the electrode is charged, while the total capacitance at the point of zero charge (PZC) maintains a similar level[49]. Based on the band theory calculation of few-layer graphene, a decreased number of graphene layers leads to an increased electrostatic interaction between graphene electrons and electrolyte ions due to lack of electrostatic charge screening, resulting in an elevated EDL capacitance (i.e., Helmholtz capacitance). Using a similar approach, Uesugi et al. estimated the total capacitance of graphene using two-terminal field-effect transistors with DC/AC power supplies and showed that the quantum capacitance dominates the total capacitance of graphene when the number of layers is less than four (Fig. 5d)[50]. As the number of graphene layers increases beyond four layers, the total capacitance saturates despite the elevated quantum capacitance because of effective screening through the EDL and first 3–4 layers of graphene (Fig. 5e). On the other hand, Zhan and Jiang demonstrated an electrostatic potential drop through a series of interfacial capacitors using joint density functional theory (JDFT)[51]. Their simulation indicated that the contribution of dielectric screening in few-layer graphene becomes increasingly dominant as the number of layers increases to more than three, whereas the potential drop in the EDL capacitance is not strongly correlated with the number of graphene layers.

Similar to the wetting phenomena of 2D materials, the formation of EDLs is affected by adventitious hydrocarbon contamination from the air and liquid. There have been several reports about the time-dependent degradation of the total capacitance of HOPG attributed to the formation of a dielectric dead layer on the HOPG surface. Zou et al. reported that freshly exfoliated HOPG (FEG) exhibited a higher total capacitance than HOPG aged for 24 h in air (AAG) or in inert gas (IAG), which is

consistent with the increase in the WCA of aged HOPGs (Fig. 5f)[52]. Hurst et al. also described the hydrocarbon contamination in both the gas and liquid phase[53]. Even highly purified deionized water causes monolayer deposition of a hydrocarbon layer ($t \sim 0.5$ nm) on a HOPG surface, which degrades the total capacitance of the HOPG. Duignan and Zhao conducted quantum mechanical calculations that explained that the anomalously low experimental capacitance observed in graphene, few-layer graphene, HOPG and activated carbon is a consequence of a dielectric dead layer comprising hydrocarbon contaminants[54].

Given the precise control and growing understanding of the EDL over graphene, graphene-based EDL capacitors are becoming a promising candidate for energy storage applications. For this application, additional attention has been paid to improving the quantum capacitance rather than the EDL capacitance because quantum capacitance is tunable by changing the density of states of graphene. This tuning of the quantum capacitance has been experimentally and theoretically examined by varying the topological defects, dopants, and chemical functionalization. One can find several comprehensive review papers regarding energy storage via graphene EDL capacitors[55–57].

While the energy storage applications of EDL capacitors are based on static ion distributions at the graphene interface, the dynamic redistribution of ions resulting from a moving electrolyte or graphene layer provides interesting opportunities for energy harvesting using EDL capacitors[58–60]. Figure 6a schematically illustrates how the drawing potential is generated by a graphene EDL-based energy harvester. The motion of liquid droplets entrains double layer ions and changes the ion distribution on the graphene surface from a static to a dynamic state (Fig. 6b). As a consequence, the front and rear of the moving droplet simultaneously charge and discharge the EDL capacitor, respectively, leading to an electric current. The generated electricity is controlled by the flow direction and velocity, as shown in Fig. 6c, as well as other factors, such as the number of droplets and the number of layers. Other than the drawing potential, there are several different electropotential-driven energy harvesting mechanisms, such as the streaming potential, waving potential, evaporation potential, and moisture-induced electricity, which are summarized in review articles[60–62].

The EDL of graphene has also been applied to sensing applications for liquid flow, ion concentration, and biomolecules[63–66]. Solution-gated graphene FETs are reported to sense flow velocity in microfluidic channels by measuring the streaming potential[63,64]. Figure 6d illustrates how the flow of an electrolyte entrains ions in the double layer and causes a streaming potential between two separate sensing channels in a six-probe graphene FET. The streaming potential can be measured by a shift in the point of zero charge in the transfer curves, which is strongly affected by the flow rate and ionic strength of the electrolyte (Fig. 6e). In the same vein, various biomolecules in an electrolyte change the relative potential drop in gate and channel EDLs because of electro-oxidization of molecules near the gate and resultant Faradic current (Fig. 6f)[65]. According to the work from Zhang et al., a shift in the Dirac point is highly sensitive to the presence of dopamine, where only 1 nM of dopamine in PBS electrolyte is detectable in graphene EDL-based sensors (Fig. 6g).

Frictional interaction between liquids and 2D materials

In addition to a modulation in the WCA and EDL, 2D material–liquid interactions have a profound influence on the friction and surface adhesion. Before the advent of atomically thin materials via mechanical exfoliation in 2004, van der Waals layered materials, such as graphite and MoS_2, were widely acknowledged as solid lubricants upon the application of a shear force due to basal plane sliding that results from a weak interlayer bond, strength[67]. When these layered materials are thinned down to less than a few atomic-layers, unique mechanical and interfacial properties emerge and start to govern the nanoscale frictional behavior, which has a bearing on the macroscopic friction performance. There are several aspects of the solid-state friction of 2D materials, such as the puckering effect, reversible slippage, layer-number dependence, and friction hysteresis, which are summarized in several review articles[68–70]. While solid-to-solid lubrication of 2D materials attracted attention at the early stage of low-dimensional tribology studies, the frictional interaction of liquid molecules with atomically thin substrates (i.e., hydrofriction) has recently become an intriguing research area for the fundamental science of solid–liquid interfaces as well as for technological applications in nanofluidics, water filtration, desalination membranes, and energy harvesting.

In general, macroscopic Newtonian flow restricts the motion of liquid molecules at solid–liquid interfaces, but nanoconfined liquid molecules have a particular structure near the interface and experience motion along the surface, which is characterized by the slip length and ratio between the liquid viscosity and interfacial friction. The unique hydrofrictional behavior of nanoconfined liquids exemplifies the extremely large liquid viscosity and wettability-dependent slip length of various surfaces[71–73]. For instance, carbon nanotubes (CNTs) have a very large slip length of more than several hundred nanometers that allows almost frictionless water flow through nanotube channels[74].

Regarding the friction of nanoconfined water molecules on 2D materials, there are several factors to be considered beyond the wettability, such as energy corrugation,

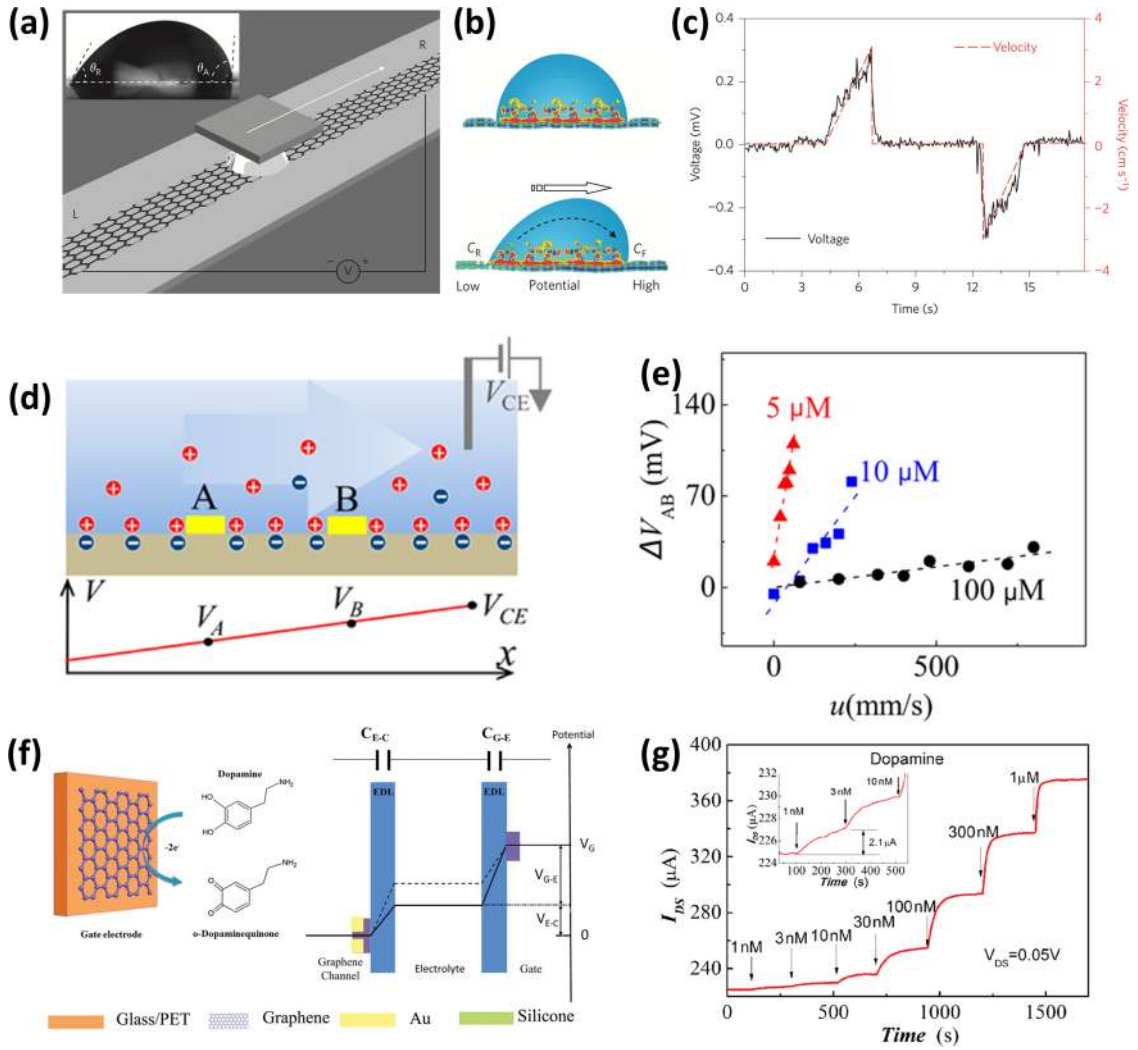

Fig. 6 Various applications of electrical double layers on graphene. a–c Energy harvesting by generating a drawing potential at electrolyte-graphene interfaces. **a** Schematic diagram of an energy harvester composed of an electrolyte droplet sandwiched by graphene and a SiO_2/Si wafer. **b** Formation of pseudocapacitors on graphene under static (upper) and dynamic (bottom) conditions. **c** Electricity generation, which is proportional to the velocity of electrolyte droplets[58]. **d**, **e** Flow rate and ionic concentration sensor of a six-channel graphene FET in ionic solution. **d** Schematic illustration of the varied ionic distribution in channels A and B due to streaming potential entrained by liquid flow. **e** Streaming potential difference between channels A and B as a function of flow rate and ionic concentration. **f**, **g** Biomolecule sensors based on solution-gated graphene transistors[64]. **f** Schematic diagram of the electrochemical reaction between dopamine and graphene, resulting in changes in the EDL potential distribution. **g** Source/drain current measurement as a function of dopamine concentration. Note that only 1 nM dopamine is sufficient for generating a different channel response[65]. **a–c** Republished with permission of Springer Nature from Yin et al.[58], permission conveyed through the Copyright Clearance Center, Inc. **d**, **e** Reprinted (adapted) with permission from Newaz et al.[64], Copyright (2012) from the American Chemical Society[64]. **f**, **g** Republished with permission of John Wiley and Sons from Zhang et al.[65], permission conveyed through the Copyright Clearance Center, Inc.

electrostatic interaction and electrolyte ions, which affect the friction of liquid molecules. Tocci et al. reported that graphene and h-BN have a similar wettability, but h-BN exhibited a water friction coefficient three times higher than graphene and a slip length one third that of graphene (Fig. 7a)[75]. This difference was attributed to the higher corrugation in the potential energy landscape of h-BN because of the heterogeneous composition of h-BN and distinct water dipole configuration in each valley. Rajan et al. also determined the wettability and friction between the h-BN basal plane and three different liquid molecules (i.e., water, ethylene glycol, and diiodomethane) by means of MD simulation[76]. Calculating the dispersion force and the electrostatic force between the h-BN and liquid molecules revealed that the wettability is dominated by dispersion relations, but the frictional coefficient depends

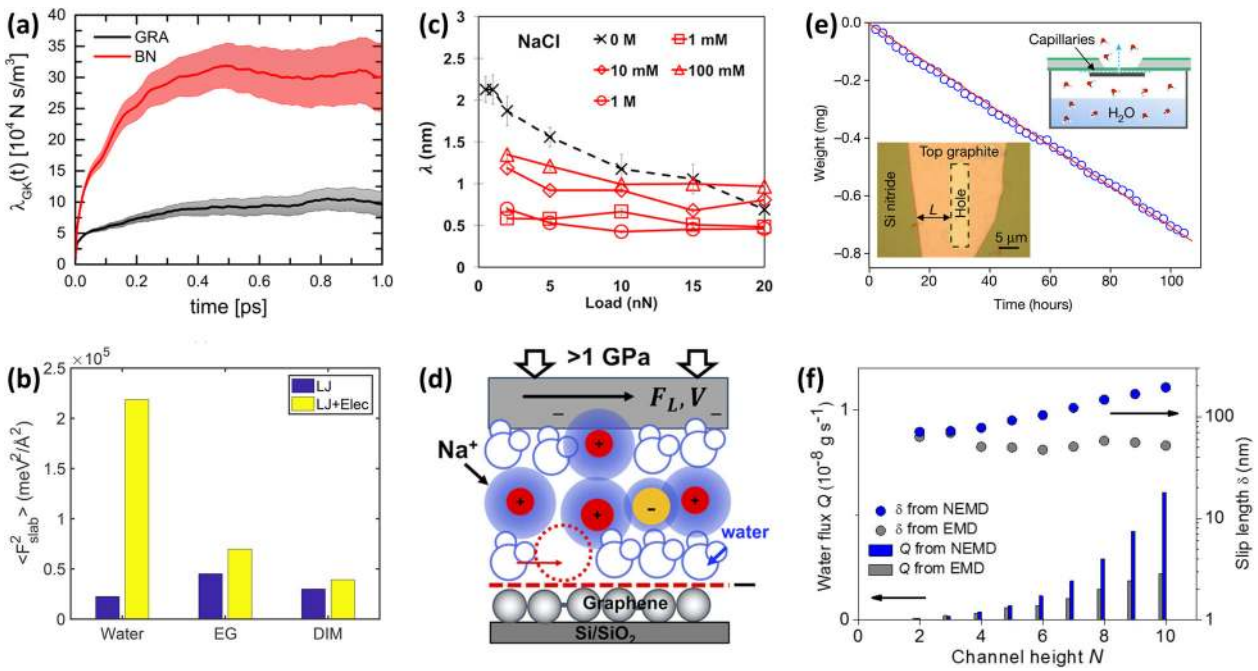

Fig. 7 Friction between liquid molecules and atomically thin materials. a Friction coefficient of water molecules on graphene and h-BN estimated by molecular dynamics and the Green–Kubo relation. The three-fold increase in the friction coefficient in the h-BN/water system results from the corrugated free energy profile on h-BN compared to the graphene/water system[75]. **b** Mean squared lateral force of water, ethylene glycol (EG), and diiodomethane (DIM) on the h-BN surface, with and without consideration of electrostatic interaction (Elec). A large deviation between LJ (dispersion only) and LJ + Elec appeared only in water, resulting in a large friction coefficient with low wettability[76]. **c** Shear activation length of an NaCl aqueous solution as a function of ionic strength and applied load. **d** Schematic illustration of water slip on the graphene surface in the presence of solvated ions in the electrical double layer[77]. **e** Water weight loss over time due to nanoscale graphene capillary channel as described in the schematic cartoon and optical images. **f** Water flux and slip length as a function of capillary channel height estimated by molecular dynamics simulation[78]. **a** Reprinted (adapted) with permission from Tocci et al.[75], Copyright (2014) American Chemical Society. **b** Reprinted (adapted) with permission from Rajan et al.[76], Copyright (2019) American Chemical Society. **c**, **d** Reprinted (adapted) with permission from Diao et al.[77], Copyright (2019) American Chemical Society. **e**, **f** Republished with permission of Springer Nature from Radha et al.[78], permission conveyed through the Copyright Clearance Center, Inc[78].

on electrostatic interactions between h-BN and polar molecules, particularly water (Fig. 7b). As a result, they showed a nonintuitive result that water has low wettability (i.e., a high WCA) but a high friction coefficient on h-BN due to strong electrostatic interactions.

The presence of electrolyte ions is crucial for the application of graphene-based nanochannels toward energy harvesting and desalination/ion filtering membranes. However, research on the effect of dissolved ions on the friction over 2D materials has been limited. Diao et al. recently estimated the slip behavior of NaCl and KCl aqueous solutions with varied ionic concentrations by means of liquid phase AFM[77]. They showed that the slipperiness of water molecules on graphene is reduced by electrolyte cations in the electrical double layer on graphene, resulting in a decreased shear-activation length, as shown in Fig. 7c. This behavior is also dependent on the electrolyte composition, where preferential adsorption of hydrated Na^+ ions causes a conspicuous modulation of the thermal activation energy for slip and therefore the friction force (Fig. 7d).

In contrast to the results from previous theoretical studies and AFM measurements, there are device-scale graphene nanofluidic channels through which water molecules flow with low friction and large slip. Rahda et al. developed a van der Waals assembly of graphene nanochannels with a layer-determined spacer and investigated capillary mass transport through the channel as a function of channel dimensions (Fig. 7e)[78]. They showed that even several tens of atomic planes enable an extraordinarily fast water transport rate (~1 m/s), which was attributed to the high capillary pressure and large slip length of the nanoconfined water molecules in the channel (Fig. 7f). Recently, the same group developed angstrom-scale nanochannels made of graphite and h-BN in which the motion of an ionic liquid was nonlinearly controlled by an external pressure and electrical gating[79]. On the other hand, Xie et al. investigated capillary

nanofluidic channels with graphene coated on three silica side walls[80]. The slip length was experimentally estimated to range from 0 to 200 nm with a median length of 16 nm, while the value showed a low correlation to the channel height. A theoretical calculation of nanochannel water transport was also performed by Jin et al. with graphene-coated Cu nanochannels[81]. The water transport improved as the number of graphene layers increased to more than three, and this result was accounted for by the decreased water dipole relaxation time and hydrogen bonding lifetime that allow an increased water mobility as well as a decreased contribution from the underlying Cu channel to the corrugated potential barriers.

Outlook: modulation of the chemical reactivity at liquid interfaces

We have presented key areas of research on the interaction between 2D materials and liquids, including the modulation of the hydrophobic/hydrophilic behavior, EDL, and friction/adhesion. However, to date, there have been limited studies on the modulation of the chemical reactivity of 2D materials at the liquid interface, where atomically thin materials possess substantial potential for use as future catalytic platforms, such as for the hydrogen evolution reaction (HER) and electrochemical sensors[82] in biosensor and bioelectronics applications. The ability to tune the electron transfer chemistry of 2D materials at the liquid interface offers opportunities to modulate the chemical reactivity.

The chemical functionalization of graphene with particular functional groups, such as aryl diazonium molecules, is the simplest and most widely utilized method for engineering the electron transfer chemistry of graphene[83]. Covalently bonded diazonium molecules lead to distinct electron transfer characteristics that subsequently influence the chemical reactivity. However, the inability to precisely control the concentration and distribution of functional sites across the graphene surface results in a limited area and functional site-specific reactions, effectively limiting the degree of subsequent chemical reactions with targets of interest.

The rate of this functionalization can be affected by the supporting substrate[84,85], presence of defects and grain boundaries[85], and presence of mechanical strain[86], much in the same way the wettability, EDL, and friction/adhesion are modulated. The supporting substrate can affect the chemical reactivity due to the substrate-induced charge fluctuation in graphene, forming charge unbalanced areas termed electron-hole puddles[87]. Other studies suggested that the chemical reactivity of graphene is more activated along the edge than the basal plane due to the existence of dangling bonds[88], but this type of defect engineering has challenges in the size and spatial distribution control. Bissett et al. investigated the change in the reaction rate of the functionalization of diazonium molecules that emerged in aqueous solution while applying a mechanical strain[86]. Mechanical strains alter the density of states (DOS) and Fermi level of graphene, resulting in a modification of the redox potential of the diazonium molecules and dramatically enhancing the reaction rate by a factor of up to ten[86]. A mechanical strain was demonstrated as a new type of catalyst allowing chemical reactions that would otherwise not proceed.

Most recently, it has been reported that this reactivity can be further tuned by adjusting the Fermi level by introducing a self-assembled monolayer (SAM) and different doping agents[84]. Myung et al. investigated the degree of chemical reactivity of graphene with respect to the type of subsurface dopant applied to the substrate. The degree of chemical reactivity on the graphene surface was directly governed by the type of doping. Among the different doping types, electron-rich n-type doping types exhibited the most reactivity due to the increased donation of electrons. This n-doped graphene was further utilized as a growth template for gold particles, which further enhanced the electrochemical reactivity, enabling its use as an atomically thin catalytic platform in an aqueous environment. The electrochemical reaction of graphene with respect to the Fermi level was assessed by the HER upon immersion in sulfuric acid electrolyte. Free electrons from the gold particles triggered additional n-doping, which facilitated the electron transfer from graphene by lowering the potential barriers for hydrogen reduction. All these studies suggest that modulating the electron transfer chemistry of 2D materials enables the use of 2D materials as a platform for controlled chemical reactions at liquid interfaces and potential future applications, such as catalytically active surfaces and novel electrochemical sensors.

Conclusion

In conclusion, liquid interactions at the surface of 2D materials are of great interest and provide opportunities for the control of interfacial properties; tuning of electronic structures, adhesion and friction; and production of novel chemical interactions. The inherent wetting behavior of 2D materials is perturbed by complexed molecules and the underlying substrate, which can be used to tune the wettability. This ability to control the spreading of liquids across a 2D material surface permits control of cellular and crystal growth, filtration, and actuation. In addition, modulation of the wettability correlates with a modification of the inherent EDL over 2D materials, altering the electrostatic interactions and allowing for the development of nanojunction gating and supercapacitor devices for energy storage and harvesting. Perturbation of the interfacial liquid structure via modification of the EDL has implications beyond electrostatic modulation, such as

constraining the liquid flow across the surface, which modifies the hydrofrictional behavior of the fluids passing through channels and across surfaces. Implications of the interactions between liquids and 2D materials are still emerging. For instance, enhanced electron transfer, enabled by modulating the wetting of graphene offers new routes to efficiently functionalize graphene for catalytic and particle growth surfaces in aqueous solutions. Indeed, with the ever-growing library of 2D materials and their application in liquid phase sensors, actuators, and surface modifiers, establishing our understanding of the interaction of 2D materials and liquids has never been more important.

Acknowledgements

P.S. and C.C. gratefully acknowledge support from the NASA Space Technology Research Fellowship (NNX16AM69H and 80NSSC17K149). S.N. gratefully acknowledges support from the NSF (DMR-1708852, MRSEC DMR-1720633, and CMMI-1554019), DTRA (HDTRA1620298), NASA ECF (NNX16AR56G), ONR YIP (N00014-17-1-2830) and AFOSR (FA9550-16-1-0251, and FA2386-17-1-4071). This research was partially supported by the NSF through the University of Illinois at Urbana-Champaign Materials Research Science and Engineering Center DMR-1720633.

Conflict of interest

The authors declare that they have no conflict of interest.

Received: 12 July 2019 Revised: 9 December 2019 Accepted: 19 January 2020.
Published online: 13 March 2020

References

1. Hirasaki, G. J. Wettability: fundamentals and surface forces. *SPE Form. Eval.* **6**, 217–226 (1991).
2. Quéré, D. Wetting and roughness. *Annu. Rev. Mater. Res.* **38**, 71–99 (2008).
3. Li, Z. et al. Effect of airborne contaminants on the wettability of supported graphene and graphite. *Nat. Mater.* **12**, 925 (2013).
4. Geim, A. K. Graphene: status and prospects. *Science* **324**, 1530–1535 (2009).
5. Goniszewski, S. et al. Correlation of p-doping in CVD Graphene with Substrate Surface Charges. *Sci. Rep.* **6**, 22858 (2016).
6. Wang, M. C. et al. Mechanical instability driven self-assembly and architecturing of 2D materials. *2D Mater.* **4**, 022002 (2017).
7. Kozbial, A., Zhou, F., Li, Z., Liu, H. & Li, L. Are graphitic surfaces hydrophobic? *Acc. Chem. Res.* **49**, 2016 (2016).
8. Wang, S., Zhang, Y., Abidi, N. & Cabrales, L. Wettability and surface free energy of graphene films. *Langmuir* **25**, 11078–11081 (2009).
9. Raj, R., Maroo, S. C. & Wang, E. N. Wettability of graphene. *Nano Lett.* **13**, 1509–1515 (2013).
10. Suzuki, S. et al. Benzene forms hydrogen bonds with water. *Science* **257**, 942–945 (1992).
11. Wu, Y. & Aluru, N. R. Graphitic carbon-water nonbonded interaction parameters. *J. Phys. Chem. B* **117**, 8802–8813 (2013).
12. Hong, G. et al. On the mechanism of hydrophilicity of graphene. *Nano Lett.* **16**, 4447–4453 (2016).
13. Liu, J., Lai, C. Y., Zhang, Y. Y., Chiesa, M. & Pantelides, S. T. Water wettability of graphene: interplay between the interfacial water structure and the electronic structure. *RSC Adv.* **8**, 16918–16926 (2018).
14. Liu, H. & Li, L. Graphitic materials: intrinsic hydrophilicity and its implications. *Extrem. Mech. Lett.* **14**, 44–50 (2017).
15. Van Engers, C. D. et al. Direct measurement of the surface energy of graphene. *Nano Lett.* **17**, 3815–3821 (2017).
16. Hamada, I. Adsorption of water on graphene: a van der Waals density functional study. *Phys. Rev. B* **86**, 1–6 (2012).
17. Feng, J. & Guo, Z. Wettability of graphene: from influencing factors and reversible conversions to potential applications. *Nanoscale Horiz.* **4**, 339–364 (2019).
18. Kozbial, A., Gong, X., Liu, H. & Li, L. Understanding the intrinsic water wettability of molybdenum disulfide (MoS2). *Langmuir* **31**, 8429–8435 (2015).
19. Kozbial, A. et al. Study on the surface energy of graphene by contact angle measurements. *Langmuir* **30**, 8598–8606 (2014).
20. Rafiee, J. et al. Wetting transparency of graphene. *Nat. Mater.* **11**, 217 (2012).
21. Parobek, D. & Liu, H. Wettability of graphene. *2D Mater.* **2**, 032001 (2015).
22. Shih, C. et al. Breakdown in the wetting transparency of graphene. *Phys. Rev. Lett.* **109**, 176101 (2012).
23. Annamalai, M. et al. Surface energy and wettability of van der Waals structures. *Nanoscale* **8**, 5764–5770 (2016).
24. Kong, W. et al. Polarity governs atomic interaction through two-dimensional materials. *Nat. Mater.* **17**, 999 (2018).
25. Lu, J. Y. et al. Insights into graphene wettability transparency by locally probing its surface free energy. *Nanoscale* **11**, 7944–7951 (2019).
26. Chow, P. K. et al. Wetting of mono and few-layered WS2 and MoS2 films supported on Si/SiO2 substrates. *ACS Nano* **9**, 3023–3031 (2015).
27. Peng, Z., Yang, R., Kim, M. A., Li, L. & Liu, H. Influence of O2, H2O and airborne hydrocarbons on the properties of selected 2D materials. *Rsc Adv.* **7**, 27048–27057 (2017).
28. Lu, J. Y., Lai, C. Y., Almansoori, I. & Chiesa, M. The evolution in graphitic surface wettability with first-principles quantum simulations: the counterintuitive role of water. *Phys. Chem. Chem. Phys.* **20**, 22636–22644 (2018).
29. Ashraf, A. et al. Spectroscopic investigation of the wettability of multilayer graphene using highly ordered pyrolytic graphite as a model material. *Langmuir* **30**, 12827–12836 (2014).
30. Aria, A. I. et al. Time evolution of the wettability of supported graphene under ambient air exposure. *J. Phys. Chem. C.* **120**, 2215–2224 (2016).
31. Ashraf, A. et al. Doping-induced tunable wettability and adhesion of graphene. *Nano Lett.* **16**, 4708–4712 (2016).
32. Tian, T. et al. Doping-driven wettability of two-dimensional materials: a multiscale theory. *Langmuir* **33**, 12827–12837 (2017).
33. Ren, H. et al. Interfacial structure and wetting properties of water droplets on graphene under a static electric field. *Phys. Chem. Chem. Phys.* **17**, 23460–23467 (2015).
34. Shahini, A., Zeng, P., Zhao, Y. & Cheng, M. M. C. Individually tunable liquid lens arrays using transparent graphene for compound eye applications. in *Proc. IEEE Int. Conf. Micro Electro Mech. Syst*. 597–600 (2016). https://doi.org/10.1109/MEMSYS.2016.7421696.
35. Pu, J. et al. Controlled water adhesion and electrowetting of conducting hydrophobic graphene/carbon nanotubes composite films on engineering materials. *J. Mater. Chem. A* **1**, 1254–1260 (2013).
36. Zhang, Z.-Q. et al. Wetting and motion behaviors of water droplet on graphene under thermal-electric coupling field. *J. Appl. Phys.* **117**, 074304 (2015).
37. Wan, S., Pu, J., Zhang, X., Wang, L. & Xue, Q. The tunable wettability in multistimuli-responsive smart graphene surfaces. *Appl. Phys. Lett.* **102**, 011603 (2013).
38. Xu, Z. et al. Reversible hydrophobic to hydrophilic transition in graphene via water splitting induced by UV irradiation. *Sci. Rep.* **4**, 6450 (2014).
39. Gaur, A. P. S. et al. Surface energy engineering for tunable wettability through controlled synthesis of MoS2. *Nano Lett.* **14**, 4314–4321 (2014).
40. Choi, J. et al. Hierarchical, dual-scale structures of atomically thin MoS2 for tunable wetting. *Nano Lett.* **17**, 1756–1761 (2017).
41. Nayak, T. R. et al. Graphene for controlled and accelerated osteogenic differentiation of human mesenchymal stem cells. *ACS Nano* **5**, 4670–4678 (2011).
42. Zhang, L. et al. Janus graphene from asymmetric two-dimensional chemistry. *Nat. Commun.* **4**, 1443–1447 (2013).
43. Ng, S. W., Noor, N. & Zheng, Z. Graphene-based two-dimensional Janus materials. *NPG Asia Mater.* **10**, 217 (2018).
44. Nguyen, N. N. et al. Atomically thin epitaxial template for organic crystal growth using graphene with controlled surface wettability. *Nano Lett.* **15**, 2474–2484 (2015).
45. Celebi, K. et al. Ultimate permeation across atomically thin porous graphene. *Sci. (80-.)* **344**, 289–292 (2014).

46. Xia, J., Chen, F., Li, J. & Tao, N. Measurement of the quantum capacitance of graphene. *Nat. Nanotechnol.* **4**, 505–509 (2009).
47. Kwon, S. S. et al. Electrical double layer of supported atomically-thin materials. *Nano Lett.* **19**, 4588–4593 (2019).
48. Yang, H. et al. Substrate effects in graphene-based electric double-layer capacitors: the pivotal interplays between ions and solvents. *ChemElectroChem* **4**, 2966–2974 (2017).
49. Ji, H. et al. Capacitance of carbon-based electrical double-layer capacitors. *Nat. Commun.* **5**, 3317 (2014).
50. Uesugi, E., Goto, H., Eguchi, R., Fujiwara, A. & Kubozono, Y. Electric double-layer capacitance between an ionic liquid and few-layer graphene. *Sci. Rep.* **3**, 1595 (2013).
51. Zhan, C. & Jiang, D. E. Contribution of dielectric screening to the total capacitance of few-layer graphene electrodes. *J. Phys. Chem. Lett.* **7**, 789–794 (2016).
52. Zou, Y., Walton, A. S., Kinloch, I. A. & Dryfe, R. A. W. Investigation of the differential capacitance of highly ordered pyrolytic graphite as a model material of graphene. *Langmuir* **32**, 11448–11455 (2016).
53. Hurst, J. M., Li, L. & Liu, H. Adventitious hydrocarbons and the graphite-water interface. *Carbon N. Y* **134**, 464–469 (2018).
54. Duignan, T. T. & Zhao, X. S. Impurities limit the capacitance of carbon-based supercapacitors. *J. Phys. Chem. C.* **123**, 4085–4093 (2019).
55. Mendoza-Sánchez, B. & Gogotsi, Y. Synthesis of two-dimensional materials for capacitive energy storage. *Adv. Mater.* **28**, 6104–6135 (2016).
56. Zhan, C. et al. Computational insights into materials and interfaces for capacitive energy storage. *Adv. Sci.* **4**, 1700059 (2017).
57. Zhang, L. L. & Zhao, X. S. Carbon-based materials as supercapacitor electrodes. *Chem. Soc. Rev.* **38**, 2520–2531 (2009).
58. Yin, J. et al. Generating electricity by moving a droplet of ionic liquid along graphene. *Nat. Nanotechnol.* **9**, 378–383 (2014).
59. Yin, J. et al. Waving potential in graphene. *Nat. Commun.* **5**, 1–6 (2014).
60. Zhang, Z. et al. Emerging hydrovoltaic technology. *Nat. Nanotechnol.* **13**, 1109–1119 (2018).
61. Tang, Q. & Yang, P. The era of water-enabled electricity generation from graphene. *J. Mater. Chem. A* **4**, 9730–9738 (2016).
62. Liu, G., Chen, T., Xu, J. & Wang, K. Blue energy harvesting on nanostructured carbon materials. *J. Mater. Chem. A* **6**, 18357–18377 (2018).
63. He, R. X. et al. Solution-gated graphene field effect transistors integrated in microfluidic systems and used for flow velocity detection. *Nano Lett.* **12**, 1404–1409 (2012).
64. Newaz, A. K. M., Markov, D. A., Prasai, D. & Bolotin, K. I. Graphene transistor as a probe for streaming potential. *Nano Lett.* **12**, 2931–2935 (2012).
65. Zhang, M. et al. High-performance dopamine sensors based on whole-graphene solution-gated transistors. *Adv. Funct. Mater.* **24**, 978–985 (2014).
66. Yan, F., Zhang, M. & Li, J. Solution-gated graphene transistors for chemical and biological sensors. *Adv. Healthc. Mater.* **3**, 313–331 (2014).
67. Dienwiebel, M. et al. Superlubricity of graphite. *Phys. Rev. Lett.* **92**, 1–4 (2004).
68. Berman, D., Erdemir, A. & Sumant, A. V. Graphene: a new emerging lubricant. *Mater. Today* **17**, 31–42 (2014).
69. Zhang, S., Ma, T., Erdemir, A. & Li, Q. Tribology of two-dimensional materials: From mechanisms to modulating strategies. *Mater. Today* **26**, 67–86 (2018).
70. Spear, J. C., Ewers, B. W. & Batteas, J. D. 2D-nanomaterials for controlling friction and wear at interfaces. *Nano Today* **10**, 301–314 (2015).
71. Ortiz-Young, D., Chiu, H. C., Kim, S., Voïtchovsky, K. & Riedo, E. The interplay between apparent viscosity and wettability in nanoconfined water. *Nat. Commun.* **4**, 2482 (2013).
72. Wu, K. et al. Wettability effect on nanoconfined water flow. *Proc. Natl Acad. Sci.* **114**, 3358–3363 (2017).
73. Huang, D. M., Sendner, C., Horinek, D., Netz, R. R. & Bocquet, L. Water slippage versus contact angle: a quasiuniversal relationship. *Phys. Rev. Lett.* **101**, 1–4 (2008).
74. Secchi, E. et al. Massive radius-dependent flow slippage in carbon nanotubes. *Nature* **537**, 210–213 (2016).
75. Tocci, G., Joly, L. & Michaelides, A. Friction of water on graphene and hexagonal boron nitride from Ab initio methods: Very different slippage despite very similar interface structures. *Nano Lett.* **14**, 6872–6877 (2014).
76. Govind Rajan, A., Strano, M. S. & Blankschtein, D. Liquids with lower wettability can exhibit higher friction on hexagonal boron nitride: the intriguing role of solid-liquid electrostatic interactions. *Nano Lett.* **19**, 1539–1551 (2019).
77. Diao, Y., Greenwood, G., Wang, M. C., Nam, S. W. & Espinosa-Marzal, R. M. Slippery and sticky graphene in water. *ACS Nano* **13**, 2072–2082 (2019).
78. Radha, B. et al. Molecular transport through capillaries made with atomic-scale precision. *Nature* **538**, 222–225 (2016).
79. Mouterde, T. et al. Molecular streaming and its voltage control in ångström-scale channels. *Nature* **567**, 87–90 (2019).
80. Xie, Q. et al. Fast water transport in graphene nanofluidic channels. *Nat. Nanotechnol.* **13**, 238–245 (2018).
81. Jin, Y., Tao, R. & Li, Z. Understanding flow enhancement in graphene-coated nanochannels. *Electrophoresis* **40**, 859–864 (2019).
82. Sheng, Z. H. et al. Electrochemical sensor based on nitrogen doped graphene: Simultaneous determination of ascorbic acid, dopamine and uric acid. *Biosens. Bioelectron.* **34**, 125–131 (2012).
83. Paulus, G. L. C., Wang, Q. H. & Strano, M. S. Covalent electron transfer chemistry of graphene with diazonium salts. *Acc. Chem. Res.* **46**, 160–170 (2013).
84. Park, M. J. et al. Enhanced chemical reactivity of graphene by fermi level modulation. *Chem. Mater.* **30**, 5602–5609 (2018).
85. Kaplan, A. et al. Current and future directions in electron transfer chemistry of graphene. *Chem. Soc. Rev.* **46**, 4530–4571 (2017).
86. Bissett, M. A., Konabe, S., Okada, S., Tsuji, M. & Ago, H. Enhanced chemical reactivity of graphene induced by mechanical strain. *ACS Nano* **7**, 10335–10343 (2013).
87. Wang, Q. H. et al. Understanding and controlling the substrate effect on graphene electron-transfer chemistry via reactivity imprint lithography. *Nat. Chem.* **4**, 724 (2012).
88. Sharma, R., Baik, J. H., Perera, C. J. & Strano, M. S. Anomalously large reactivity of single graphene layers and edges toward electron transfer chemistries. *Nano Lett.* **10**, 398–405 (2010).